ACS APPLIED MATERIALS & INTERFACES

Research Article

www.acsami.org

Large-Scale Production of PMMA/SWCNT Composites Based on SWCNT Modified with PMMA

Robin Anderson Fraser,[†] Karen Stoeffler,*[,‡] Behnam Ashrafi,[§] Yunfa Zhang,[§] and Benoit Simard[†]

[†]Steacie Institute for Molecular Sciences, National Research Council Canada, 100 Sussex Drive, Ottawa, Ontario K1A 0R6, Canada

[‡]Industrial Materials Institute, National Research Council Canada, 75 de Mortagne, Boucherville, Quebec J4B 6Y4, Canada

[§]Institute for Aerospace Research, National Research Council Canada, 1200 Montreal Road, Building M-3, Ottawa, Ontario K1A 0R6, Canada

ABSTRACT: In this work, a two-step method consisting of in situ polymerization of polymethyl methacrylate (PMMA) in the presence of single-walled carbon nanotubes (SWCNT), followed by the redispersion of the resulting compound in dimethylformamide (DMF), was used to fabricate SWCNT modified with PMMA (SWCNT−PMMA). Raman spectroscopy revealed that PMMA was merely wrapped around the SWCNT when raw SWCNT or purified SWCNT were used as the starting material. However, PMMA was covalently bonded to SWCNT when acid treated SWCNT (SWCNT-COOH) was used as the starting material. SWCNT−PMMA compounds were further diluted in pure PMMA by conventional melt compounding at large scale (several kilograms) to obtain transparent composites containing 0.09 wt % SWCNT. The micro- and nano-dispersion of the SWCNT in the composites were analyzed using scanning electron microscopy (SEM) and transmission electron microscopy (TEM). The thermal and mechanical properties of the composites were determined by thermal gravimetric analysis (TGA), differential scanning calorimetry (DSC), tensile testing, and Charpy impact testing. At the the low SWCNT loading studied, the tensile properties remain unchanged, whereas the impact strength improves by 20%.

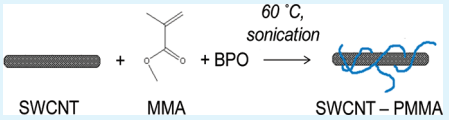

KEYWORDS: *single-walled carbon nanotubes (SWCNT), polymethyl methacrylate (PMMA), covalent functionalization, dispersion*

INTRODUCTION

In the last several years, there has been significant progress in the field of polymer/single-walled carbon nanotube (SWCNT) nanocomposites.[1] Once properly developed, polymer/SWCNT nanocomposites could have applications in a variety of industries, from textiles[2] to aerospace.[3,4] To date, SWCNT have been incorporated into several polymers with mixed results.[5,6] The two major hurdles that need to be overcome before the promise of SWCNT based nanocomposites can be realized are (1) homogeneous dispersion of SWCNT in the matrix and (2) efficient load transfer between SWCNT and the matrix.[7−9] A homogeneous dispersion is paramount as it allows for full utilization of the amazing properties[10,11] of SWCNT. Indeed, when SWCNT are aggregated in a matrix, they can cause large stress concentrations, which weaken the composite.[12]

A number of techniques, such as solution mixing or melt compounding, have been developed to incorporate SWCNT in solvents and polymer matrices. However, the poor compatibility of SWCNT with common solvents and polymers usually leads to the production of composites with aggregated SWCNT. Non-covalent wrapping of the SWCNT with a polymer or surfactant that is both compatible with SWCNT and the matrix can enhance the dispersion of SWCNT in polymer matrices. This method relies on van der Waals or electrostatic interactions between the wrapping molecule and the SWCNT. Although no damage is done to the nanotube structure (thus preserving the electronic and mechanical properties) and well-dispersed nanocomposites can be achieved, these interacting forces are inherently weaker than a covalent bond and may not result in mechanical properties enhancement for the final nanocomposite.[1] Another method to aid integration of SWCNT into a polymer matrix is functionalizing the SWCNT surface. Proper choice of functional group(s) allows one to both impart solubility to the SWCNT (in a solvent, monomer, or polymer solution) and create a covalent bond with the polymer matrix.

Toward the production of enhanced polymer/SWCNT nanocomposites, we have focused on incorporating SWCNT into polymethyl methacrylate (PMMA). PMMA-based materials are useful in practically all segments of the economy, from household to automotive products, because of their toughness, stiffness, and transparency.[13] Although less dense than the glass they usually replace, the weight of PMMA materials remains a drawback for several applications. Incorporation of reinforcing fillers, such as SWCNT, into a PMMA matrix could result in an enhanced material.

The aim of the present work is to achieve a homogeneous dispersion of SWCNT covalently bonded to the matrix via a method that can be used to fabricate composites at the industrial scale (several kilograms). To accomplish this, we have used a two-steps method. In a first step, PMMA was in situ polymerized in presence of SWCNT (Figure 1b). In a second step, the compound obtained was redispersed in a solvent in

Received: December 22, 2011
Accepted: March 15, 2012
Published: March 15, 2012

   dx.doi.org/10.1021/am201824k | *ACS Appl. Mater. Interfaces* 2012, 4, 1990−1997

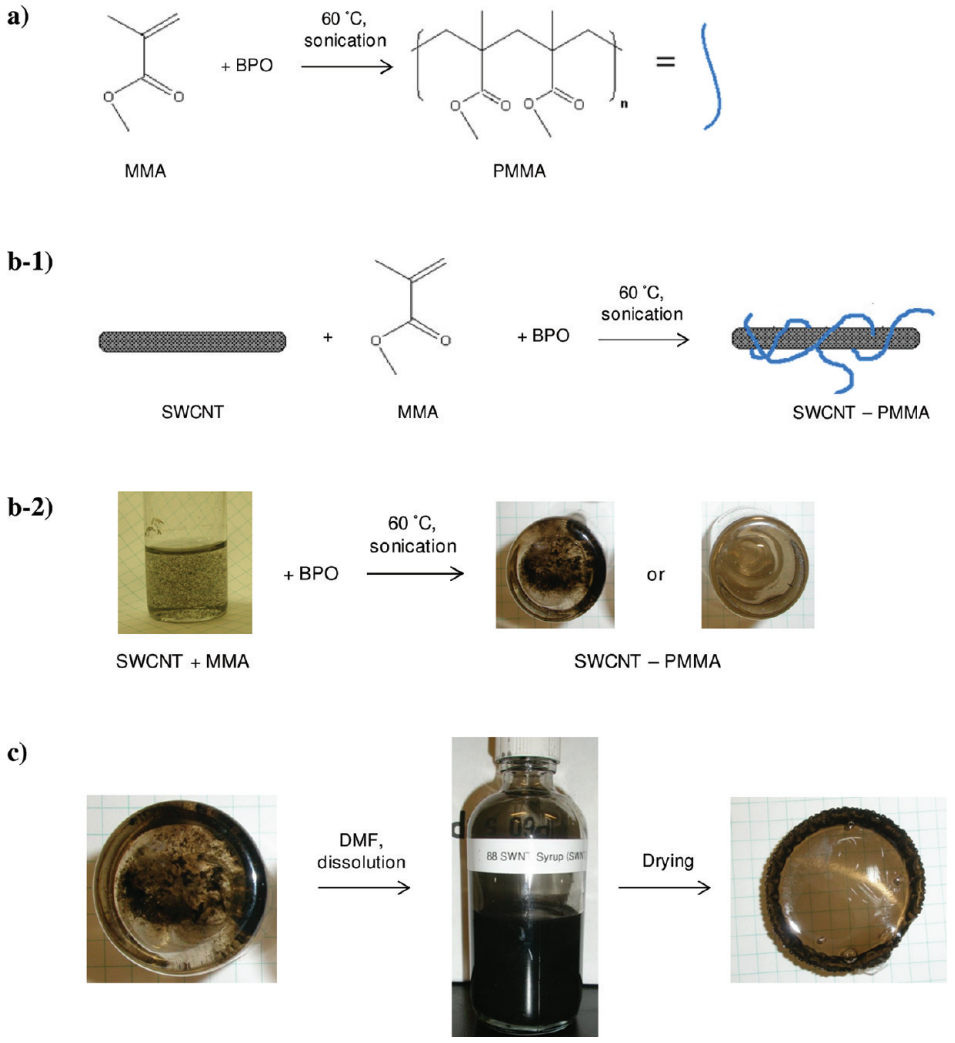

Figure 1. Fabrication of SWCNT modified with PMMA (SWCNT−PMMA): (a) in situ polymerization of PMMA; (b-1) in situ polymerization of PMMA in the presence of SWCNT (raw SWCNT, purified SWCNT, or SWCNT-COOH was used as the starting material); the resulting product is referred to as SWCNT−PMMA and has a variable dispersion; (b-2) example of results; (c) redispersion of SWCNT−PMMA in DMF in order to enhance the dispersion; after solvent removal, the final SWCNT−PMMA compound is recovered.

order to enhance the dispersion of the SWCNT by solution mixing (Figure 1c). Combining in situ polymerization and solution mixing, a composite with superior dispersion than either one of the two methods on its own could be obtained. This two-step process was used to produce large quantities of SWCNT modified with PMMA (SWCNT−PMMA) that was further diluted in pure PMMA by conventional melt compounding to produce composites at the kilogram scale.

EXPERIMENTAL SECTION

Materials. Commercial PMMA (Plexiglas V825-UVA5A; melt flow rate, 3.7 g/10 min at 230°C/3.8 kg) was obtained from Arkema (Oakville, ON). SWCNT were produced in-house by our laser ablation system.[14] Methyl methacrylate (MMA) and benzoyl peroxide (BPO) were purchased from Sigma-Aldrich. Sulfuric and nitric acids were purchased from J.T. Baker. Dimethyl formamide (DMF), hydrochloric acid, methanol, toluene, and chloroform were purchased from EMD. Hexane was purchased from Caledon Laboratories Ltd. (Georgetown, ON). Finally, ethanol was purchased from Commercial Alcohols (Brampton, ON).

Preparation of Purified SWCNT and Acid-Treated SWCNT (SWCNT-COOH). *SWCNT Purification (typical).* Raw char laser SWCNT (approximate purity: 60 %; estimated length: 3−8 μm[15]) were purified according to a methodology developed in our laboratories.[16,17] Briefly, 3.27 g of raw char laser SWCNT were suspended in 800 mL of toluene via bath sonication for 30 min. In a first step, the sample was centrifuged at 4000 rpm for 30 min and the red supernatant, containing fullerene and some amorphous carbon, was discarded. This suspension-centrifugation process was repeated 4 times with DMF to remove other amorphous carbon species. The resulting SWCNT solid was suspended in methanol to remove residual DMF, and rotovapped to dryness. In a second step, the solid was suspended in 400 mL 2 N HCl:ethanol (50:50 v/v), bath sonicated for 1 h, and stirred overnight to remove the metal catalyst contaminants. The suspension was diluted to 1 L with Millipore water, centrifuged at 8000 rpm for 30 min, and the supernatant was discarded. This procedure was repeated until the suspension reached neutral pH. In a third step, a water:hexane extraction was performed to remove silica particle contaminants. The purified SWCNT solid (approximate purity: 90 %) was suspended in methanol and rotovapped to dryness.

SWCNT-COOH Preparation (typical). The SWCNT sidewalls were functionalized with oxygen-containing groups, mainly carboxylic acid. Purified SWCNT was suspended in 800 mL sulphuric acid:nitric acid (3:1 v/v), sonicated for 1 h, and stirred overnight at 50°C. The suspension was diluted to 1 L with deionized water and filtered

Table 1. Summary of the Samples Produced

sample	SWCNT content (wt %)	fabrication process
PMMA		Reference obtained by twin-screw extrusion of PMMA.
in situ PMMA		Reference obtained by in situ polymerization of PMMA.
raw SWCNT−PMMA	0.86	Compound obtained by in situ polymerization of PMMA in presence of raw SWCNT, followed by redissolution in DMF and solvent removal.
purified SWCNT−PMMA	0.72	Compound obtained by in situ polymerization of PMMA in presence of purified SWCNT, followed by redissolution in DMF and solvent removal.
SWCNT-COOH−PMMA	0.70	Compound obtained by in situ polymerization of PMMA in presence of SWCNT-COOH, followed by redissolution in DMF and solvent removal.
PMMA/[raw SWCNT−PMMA]	0.09	Composite obtained by dilution of raw SWCNT−PMMA in pure PMMA by twin-screw extrusion.
PMMA/[purified SWCNT−PMMA]	0.09	Composite obtained by dilution of purified SWCNT−PMMA in pure PMMA by twin-screw extrusion.
PMMA/[SWCNT-COOH−PMMA]	0.09	Composite obtained by dilution of SWCNT-COOH−PMMA in pure PMMA by twin-screw extrusion.

through a 0.45 μm polycarbonate membrane. The sample was washed with deionized water until neutral pH. The yield was 2.51 g (76.8 %).

Preparation of SWCNT-Modified with PMMA (SWCNT−PMMA). *In situ PMMA (reference).* PMMA was prepared by in situ polymerization according to the method described in Figure 1a to serve as a reference material. 1.8 g BPO were dissolved in 200 mL of MMA and sonicated at 60 °C for ∼2 h until very viscous (but never boiling). The viscous suspension was poured to molds and allowed to dry overnight on a hot plate kept at 50 °C. The solid samples were removed from the aluminum molds and further dried at 120 °C under vacuum for 12 h. The final mass of the PMMA produced was ∼280 g.

SWCNT Modified with PMMA (SWCNT−PMMA). SWCNT modified with PMMA (SWCNT−PMMA) were prepared by a combination of in situ polymerization and solution mixing as shown in b and c in Figure 1. SWCNT (∼2 g) and BPO (1.8 g) were suspended in MMA (200 mL). The suspension was sonicated at 60 °C for ∼2 h until very viscous (but never boiling) using a bath sonicator Cole Palmer 8891 (input: 130 W/50−60 Hz; output, 100 W/42 kHz). The viscous suspension was poured to molds and allowed to dry overnight on a hot plate kept at 50 °C. The SWCNT−PMMA solid pieces were dissolved in the minimal amount of DMF (∼300 mL) with bath sonication (normally 1−2 h, until the solid was completely dissolved) to produce a syrup. The syrup was once again poured to molds and allowed to dry overnight on a hot plate kept at 50 °C. The solid samples were removed from the aluminum molds and further dried at 120 °C under vacuum for 12 h. Using this protocol, raw char laser SWCNT modified with PMMA (raw SWCNT−PMMA; final mass, 237.28 g; raw SWCNT content, 0.86 wt %), purified SWCNT modified with PMMA (purified SWCNT−PMMA; final mass, 251.68 g; purified SWCNT content, 0.72 wt %) and SWCNT-COOH modified with PMMA (SWCNT-COOH−PMMA; final mass, 287.96 g; SWCNT-COOH content, 0.70 wt %) were prepared.

PMMA/[SWCNT−PMMA] Composite Fabrication. Commercial PMMA and SWCNT−PMMA compounds were separately reduced into powder using a cryo-grinder. The materials were dried at 120°C for 4 h and then dry-blended in the powder state to obtain a final concentration of 0.09 wt % SWCNT. This concentration was sufficient to observe the effect of the various surface treatments while maintaining the transparency of the composites produced. In addition, it was just below the turning point in reinforcement efficiency described by Loos and Manas-Zloczower.[18] The dry-blends were fed into a Leistritz co-rotative twin-screw extruder (screw diameter, 34 mm; length, 1360 mm) operating at 220°C (die temperature) at a gravimetric flow rate of 5 kg/h and a screw speed of 100 rpm. A medium-shear screw configuration was used. The extrudate was air-cooled and pelletized. The pellets of PMMA/[SWCNT−PMMA] were vacuum dried at 90°C overnight and then compression-molded using a Carver hydraulic press (5 t) operating at 220°C to obtain flat plaques. Specimens for tensile testing and Charpy testing were further machined from those plaques. Table 1 summarizes the composition of the various composites prepared.

Characterization. *Raman Spectroscopy and Mapping.* For Raman spectroscopy, raw SWCNT, purified SWCNT, and SWCNT-COOH were suspended in methanol. A drop of the suspension was deposited on a microscope slide and the solvent was evaporated. Raw SWCNT−PMMA, purified SWCNT−PMMA, and SWCNT-COOH−PMMA syrups were directly deposited in the liquid state on a microscope slide and the solvent was evaporated. Extruded PMMA/[SWCNT−PMMA] samples were prepared by hot pressing the composite at 120 °C between two glass slides to achieve a flat surface. The samples were all ∼150 μm thick. Spectra were acquired with a Renishaw inVia spectrophotometer, using a 785 nm laser and a scanning range comprised between 100 and 3200 cm^{-1}. A minimum of 4 spectra were acquired for each sample. The intensities of the G band (at ∼1590 cm^{-1}) and D band (at ∼1300 cm^{-1}) were used to calculate the I_D/I_G ratio.

Maps were constructed using Renishaw's WiRE 3.2 software, which scans the selected 200 μm × 200 μm area by acquiring a spectrum every 2 μm in the x and y dimensions. The 785 nm laser intensity was adjusted from 0.05 to 100% depending on the material. The laser had a spot size of 1 μm and scanned the 1400 to 1800 cm^{-1} region with a 0.5 s/scan dwell time. A three-dimensional map was constructed using the % standard deviations of the areas under the G band peaks.

Electron Microscopy. Characterization of the micro-dispersion in the composites was done by scanning electron microscopy (SEM) on cryo-microtomed cross sections of the samples using a Hitachi S4700 microscope operating at 2 kV. Characterization of the submicro- and nano-dispersion was carried out by transmission electron microscopy (TEM) on cryo-ultramicrotomed sections using a JEOL JEM 2100F operating at 200 kV.

Electrical Conductivity. The electrical conductivity of the composites was measured using a high resistivity source meter Keithley 2635 with a shield to reduce noise.

Thermal Analyses. Thermal gravimetric analysis (TGA) was performed using a TA Instruments 2050 Thermogravimetric Analyzer under nitrogen gas at a rate of 10 °C/min from room temperature to 550 °C. Differential scanning calorimetry (DSC) was performed using a TA Instruments 2920 Modulated DSC under nitrogen gas at a heating rate of 5 °C/min from room temperature to 200 °C.

Tensile Testing. Uniaxial tensile loading was performed on flat, rectangular test specimen. Test specimens were machined from the compression molded plaques into 15 mm ×4 mm ×1 mm specimen bars. A mini-tensile load frame (MTI Instruments) with a 100 lb load cell was used to carry out the tests. The specimens were loaded in tension at a cross-head speed of 0.05 mm/s. The load and displacement values were recorded until specimen failure, at a sampling rate of 100 readings/s. A load drop of 50% of the peak load was taken to be the specimen failure point.

Charpy Impact Testing. Dynamic impact tests were conducted using a Charpy fixture in an Instron Dynatup 8200 instrumented drop tower. ASTM D6110 and ISO 179 standards provided the general guidance for the Charpy impact toughness test. 30 test specimens were tested in order to obtain the average impact strength. The tests were performed at ambient temperature using a penetrator impact speed of 2.45 m/s and an impact energy level of 10 J. Unnotched specimens were machined from the compression molded plaques into 12.7 mm ×12.7 mm ×127 mm specimen bars. Impact strength of unnotched specimens, a_{cU} (J/m^2), was calculated using eq 1, where w is the maximum energy absorbed by the test specimen, h is the thickness of the test specimen, and b is width of the test specimen:

$$a_{cU} = \frac{w}{bh} \quad (1)$$

RESULTS AND DISCUSSION

Raman Spectroscopy. An example of Raman spectra obtained for different types of SWCNT is shown in Figure 2.

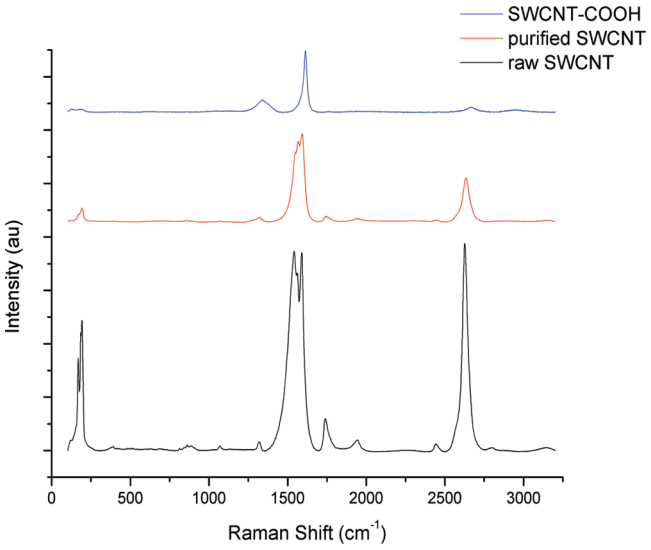

Figure 2. Raman spectra of raw SWCNT, purified SWCNT, and SWCNT-COOH.

The I_D/I_G ratios were calculated from the Raman spectra obtained. The I_D/I_G ratio is a measure of side-wall defects. Those defects can result from the SWCNT synthesis, or can have been introduced during the purification or functionalization process. As shown in Table 2, there is no significant change in the I_D/I_G ratio between raw SWCNT (0.120 ± 0.031) and purified SWCNT (0.114 ± 0.005), indicating that no damage or functionalization has occurred upon purification. As expected, the SWCNT-COOH, which have been subjected to a H_2SO_4/HNO_3 acid functionalization reaction, do indeed show an increased I_D/I_G ratio (0.230 ± 0.047) compared to that of raw SWCNT and purified SWCNT. In the SWCNT−PMMA compounds, the change in the I_D/I_G ratio observed for raw SWCNT−PMMA (0.148 ± 0.060) and purified SWCNT−PMMA (0.178 ± 0.005) was limited, when compared with raw SWCNT and purified SWCNT, respectively. This indicates that PMMA is merely wrapping around the SWCNT. On the opposite, a large increase in I_D/I_G ratio was observed for SWCNT-COOH−PMMA (0.481 ± 0.059), indicating that in this case, the PMMA is not merely wrapping around the SWCNT, but is covalently bonded to the SWCNT surface.

Table 2. Raman Spectral Data Comparing the Various SWCNT and Their Corresponding SWCNT−PMMA Compounds

sample	SWCNT content (wt %)	I_D/I_G
raw SWCNT	100	0.120 ± 0.031
raw SWCNT−PMMA	0.86	0.148 ± 0.060
purified SWCNT	100	0.114 ± 0.005
purified SWCNT−PMMA	0.72	0.178 ± 0.005
SWCNT-COOH	100	0.230 ± 0.047
SWCNT-COOH−PMMA	0.70	0.481 ± 0.059

The distribution of SWCNT in the final composites was characterized using Raman spectroscopy mapping. Simply plotting the G band intensities collected over the 200 μm × 200 μm map area is an insufficient method of analysis for distribution of SWCNT, as it is only qualitative and does not allow conclusive comparisons to be drawn between maps. Even if the distribution quality appears equivalent across the map area, comparing composites with differing signal intensities (caused by, for example, different SWCNT loadings, surface treatments, matrices, flatness, and thickness of the samples) is challenging and may be misleading. For these reasons, we employed a more quantitative method of analyzing the data collected in mapping experiments. This method is based on that described by F. Du et al.[19] It involves first obtaining the areas under the G band for all spectra and then calculating the average intensity. The intensities are then normalized to 100. This normalized data can be plotted as shown in Figure 3. This data can be further processed to calculate the standard deviation of the normalized intensity (SD, in %) which can provide a semi-quantitative description of uniformity. This is particularly appropriate if the intensity fluctuates about a constant value. In this way, a numerical value can be obtained to describe the distribution of the SWCNT in the sample. From Table 3, it can be seen that the SD value is much lower in the PMMA/[SWCNT-COOH−PMMA] composite (~22 %) than in PMMA/[raw SWCNT−PMMA] (~63 %) or PMMA/[purified SWCNT−PMMA] (~41 %) composites, indicating a better distribution of the SWCNT. In addition, melt compounding by twin-screw extrusion appears to enhance the distribution of the SWCNT. This improvement is particularly significant in the case of the PMMA / [SWCNT-COOH−PMMA] composite, whose SD value decreases from ~44% before extrusion to ~22% after extrusion.

Electron Microscopy. The SWCNT−PMMA compounds were characterized by SEM and TEM. As shown in Figure 4, TEM revealed a coarser dispersion in raw SWCNT−PMMA compared to purified SWCNT−PMMA and SWCNT-COOH−PMMA. The two latter composites exhibit a fine dispersion, although the SWCNT might not be totally dispersed at the nano-level. This result is consistent with the SD values obtained from Raman spectroscopy mapping.

A SEM micrograph of the PMMA/[SWCNT-COOH−PMMA] composite, which presented the better SWCNT distribution as determined by Raman spectroscopy mapping, is shown in Figure 5. SEM confirms the good distribution of the SWCNT and indicates a fine dispersion at the microscale, with microaggregates no larger than 5 μm.

Electrical Conductivity. The electrical conductivity was found to be 1 × 10^{-10} S/cm for the PMMA/[raw SWCNT−PMMA] composite and 5 × 10^{-10} S/cm for the PMMA/[purified SWCNT−PMMA] composite. The error on the measurements was around 50% due to the high signal/noise

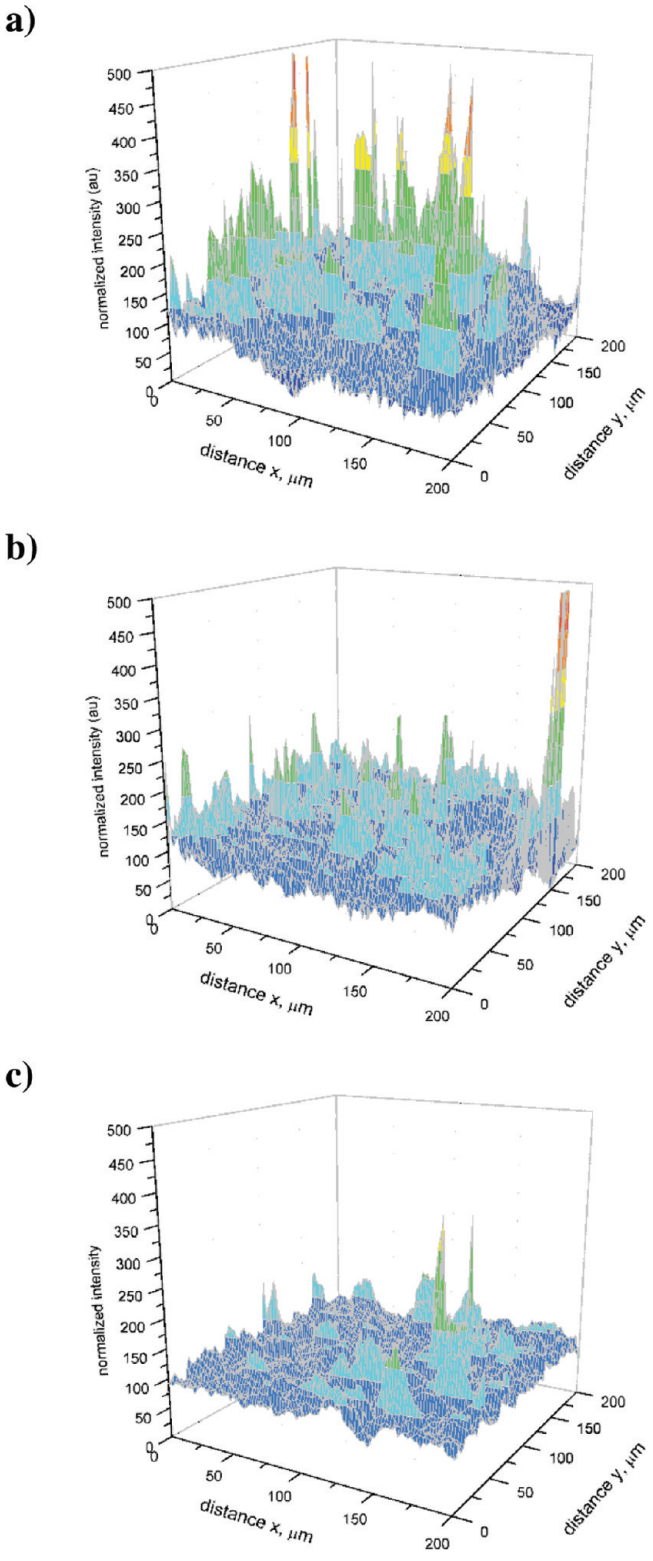

Figure 3. 3D surface plots of normalized intensity of Raman mapping signals for: (a) PMMA/[raw SWCNT−PMMA]; (b) PMMA/[purified SWCNT−PMMA]; (c) PMMA/[SWCNT−COOH−PMMA].

ratio. The low conductivity values measured are consistent with the low SWCNT content (0.09 %wt.) and the absence of a percolating network at such concentration. In addition, the increase of conductivity observed for the PMMA/[purified SWCNT−PMMA] composite is coherent with the higher purity of the SWCNT material present in the composite.

Table 3. Raman Mapping Data Comparing the Various SWCNT−SWCNT Compounds and Their Corresponding PMMA/[SWCNT−PMMA Composites]

sample	SWCNT content (wt %)	SD (%)
raw SWCNT−PMMA	0.86	69.00 ± 24.17
PMMA/[raw SWCNT−PMMA]	0.09	62.50 ± 9.52
purified SWCNT−PMMA	0.72	48.93 ± 6.25
PMMA/[purified SWCNT−PMMA]	0.09	41.20 ± 3.57
SWCNT-COOH−PMMA	0.70	44.75 ± 0.43
PMMA/[SWCNT-COOH−PMMA]	0.09	22.28 ± 4.16

Thermal Analyses. An example of TGA thermograms obtained for in situ PMMA and PMMA/[SWCNT-COOH−PMMA] is shown in Figure 6. Table 4 summarizes the temperature at 10 wt % loss ($T_{d_{10}}$) and at the maximum degradation peak ($T_{d_{peak}}$), as well as the glass transition temperature (T_g) of PMMA and its PMMA/[SWCNT−PMMA] composites, as determined by TGA and DSC. PMMA/[SWCNT−PMMA] composites show a lower degradation onset than PMMA, which should probably be attributed to the in situ PMMA fraction. However, the addition of SWCNT (0.09 wt %) allows a significant increase in $T_{d_{peak}}$ (+8 °C to +18 °C) compared to pure PMMA. Finally, DSC data do not show any improvement in T_g despite the rather good distribution and dispersion observed in the composites. This might be related to the low SWCNT content used and to an incomplete dispersion at the nanoscale, insufficient to affect the mobility of the polymer chains.

Mechanical Testing. *Tensile Testing.* The Young's modulus (E), yield stress (σ_y), tensile strength (σ_{max}), elongation at break (ε_b), and energy at break (E_b) of PMMA and PMMA/[SWCNT−PMMA] composites are summarized in Table 5. The addition of SWCNT did not improve the mechanical properties in tension compared to pure PMMA. A small reduction of Young's modulus was even measured for the PMMA/[purified SWCNT−PMMA] composite. This composite, on the other hand, offered the highest toughness as compared to the other formulations. The micromechanical modelling of Mori-Tanaka[20,21] was used to estimate the theoretical increase in Young's modulus expected for a SWCNT loading of 0.09 wt % (0.082 vol %) in a PMMA matrix. A Young's modulus of 580 GPa and aspect ratio of 1000 was considered for SWCNT arrays (bundles) randomly distributed in the matrix. Other elastic constants of SWCNT arrays necessary for this model were obtained from Popov et al.[22] A Young's modulus of 2.1 GPa and a Poisson's ratio of 0.4 were assumed for the PMMA matrix. Using those parameters, an increase of 0.16 GPa (7.6 %) in Young's modulus was estimated for a PMMA/SWCNT nanocomposite containing 0.09 wt % SWCNT. Such an increase falls within the experimental errors reported in Table 5. Therefore, higher loadings of SWCNT are needed to improve the mechanical performance of PMMA resins.

Charpy Impact Test. All specimens submitted to Charpy impact test failed in brittle fracture mode. This failure mode can be further grouped into the "one surface fracture" mode and the "multiple surface fracture" mode. A larger amount of energy is required for the "multiple surface fracture" mode. Figure 7 shows photographs of the specimens failed under those two

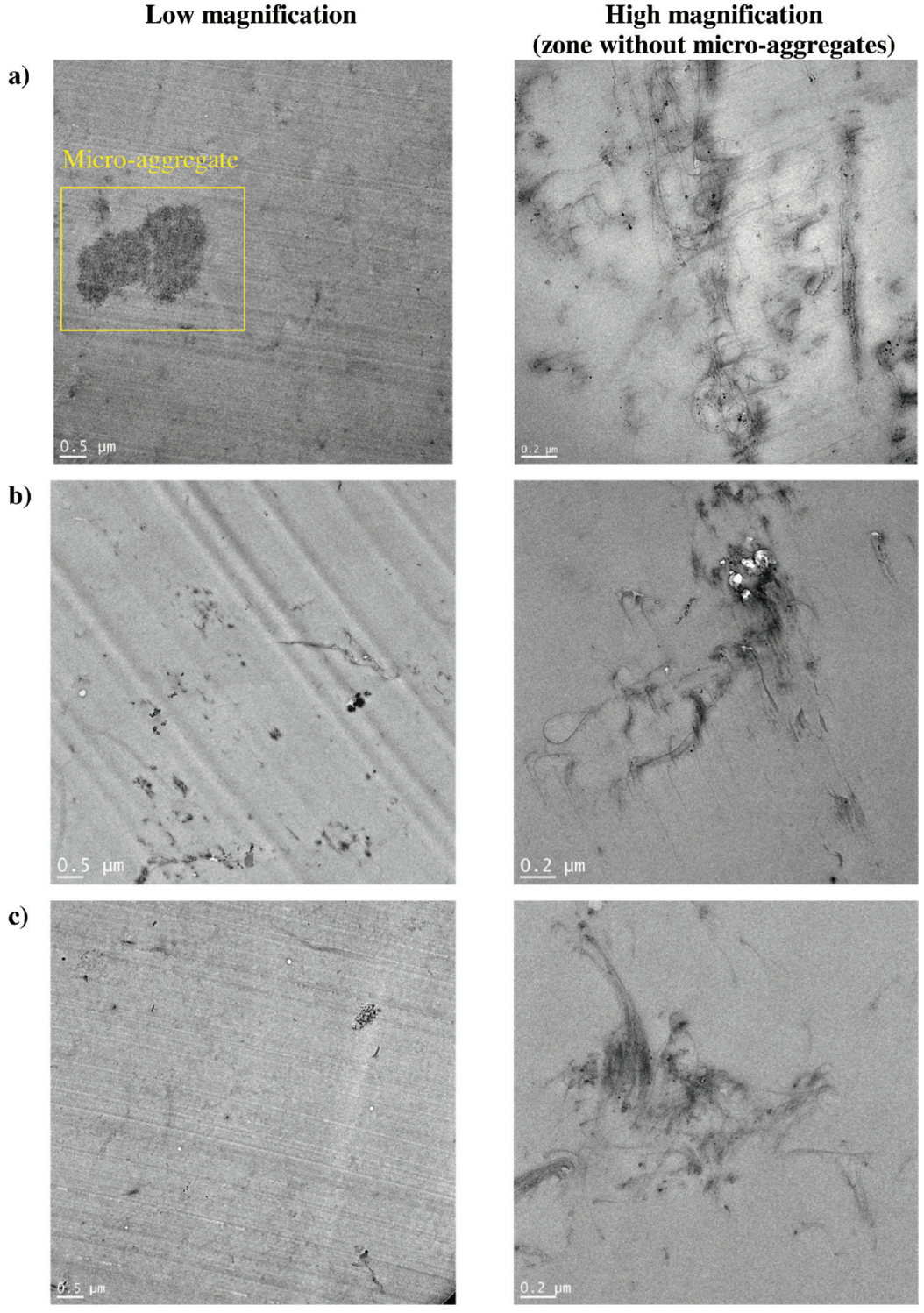

Figure 4. TEM micrographs of: (a) raw SWCNT−PMMA; (b) purified SWCNT−PMMA; (c) SWCNT-COOH−PMMA.

modes. The apparent impact strength was calculated based on the specimens failed in the "one surface fracture" mode (Table 6). A significant increase in apparent impact strength (+ 20 %) was observed for the PMMA / [SWCNT-COOH−PMMA] composite compared to pure PMMA. This may demonstrate that less SWCNT is necessary to improve the Charpy impact strength as compared to the tensile properties. However, this result should be considered carefully as the standard deviations calculated are quite high.

CONCLUSIONS

A two-step method, amenable at the industrial scale, was used to prepare SWCNT modified with PMMA. In a first step, PMMA was in situ polymerized in the presence of SWCNT. After removal of the unreacted MMA monomer, the resulting solid was redispersed in DMF to enhance the distribution and dispersion of SWCNT. After removal of the solvent, a solid compound (referred to as SWCNT−PMMA) was obtained. It was shown by Raman spectroscopy that PMMA was merely

Table 4. TGA and DSC Data of PMMA/[SWCNT−PMMA] Extruded Composites

sample	$T_{d_{10}}$ [a] (°C)	$T_{d_{peak}}$ [a] (°C)	T_g [b] (°C)
PMMA	296.3 ± 3.4	318.6 ± 0.4	107.0 ± 2.2
in situ PMMA	282.5 ± 0.6	302.6 ± 0.7	107.0 ± 0.9
PMMA/[raw SWCNT−PMMA]	283.8 ± 1.6	326.5 ± 1.2	104.5 ± 1.3
PMMA/[purified SWCNT−PMMA]	283.6 ± 1.3	327.7 ± 2.0	105.3 ± 0.1
PMMA/[SWCNT-COOH−PMMA]	283.5 ± 2.3	336.3 ± 3.7	103.6 ± 1.5

[a]Determined by TGA (N_2 atmosphere, 10 C°/min). [b]Determined by DSC (N_2 atmosphere, 5 C°/min).

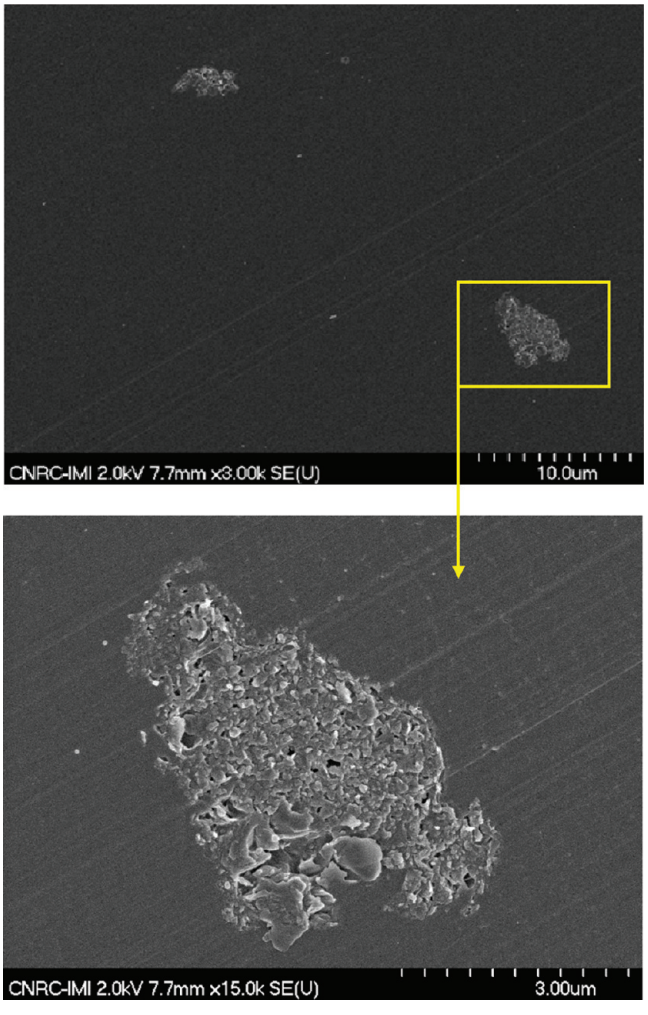

Figure 5. SEM micrographs of the PMMA/[SWCNT-COOH−PMMA] composite (microtomed surface).

wrapping around the SWCNT when raw SWCNT or purified SWCNT were used as the starting material. On the opposite, PMMA was found to be covalently bonded to SWCNT when SWCNT-COOH was used as the starting material. Furthermore, Raman mapping and TEM showed a dramatic improvement in SWCNT distribution and dispersion in SWCNT-COOH−PMMA compared to raw SWCNT−PMMA or purified SWCNT−PMMA.

SWCNT−PMMA was diluted in pure PMMA by twin-screw extrusion. PMMA/[SWCNT−PMMA] transparent composites containing 0.09 wt % SWCNT were produced at the kilogram scale. Raman mapping showed an enhancement of distribution after melt compounding. The mechanical properties in tension of the PMMA/[SWCNT−PMMA] composites were not improved compared to pure PMMA, probably because of the low SWCNT content used. However, Charpy impact testing showed a +20 % improvement over pure PMMA for the composite made using SWCNT-COOH. Greater improvements in mechanical properties in tension and under impact are expected in future composites prepared using higher SWCNT loadings.

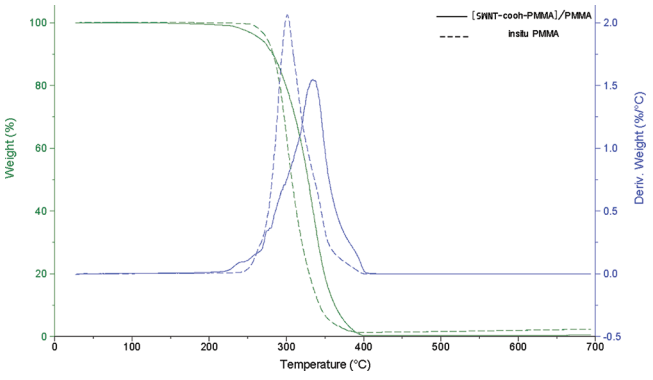

Figure 6. TGA thermograms of in situ PMMA and PMMA/[SWCNT-COOH−PMMA].

Table 5. Tensile Properties of PMMA/[SWCNT−PMMA] Extruded Composites

sample	E (GPa)	σ_y (MPa)	σ_{max} (MPa)	ε_b (%)	E_b (MPa)
PMMA	2.1 ± 0.2	37 ± 5	54 ± 5	3.8 ± 0.3	1.2 ± 0.2
in situ PMMA	2.5 ± 0.3	42 ± 3	52 ± 9	3.9 ± 1.0	1.4 ± 0.8
PMMA/[raw SWCNT−PMMA]	2.6 ± 0.3	40 ± 9	44 ± 6	2.3 ± 0.5	0.6 ± 0.2
PMMA/[purified SWCNT−PMMA]	1.8 ± 0.4	35 ± 4	46 ± 8	4.5 ± 1.1	1.4 ± 0.6
PMMA/[SWCNT-COOH−PMMA]	2.5 ± 0.9	38 ± 6	45 ± 10	2.8 ± 0.8	0.7 ± 0.4

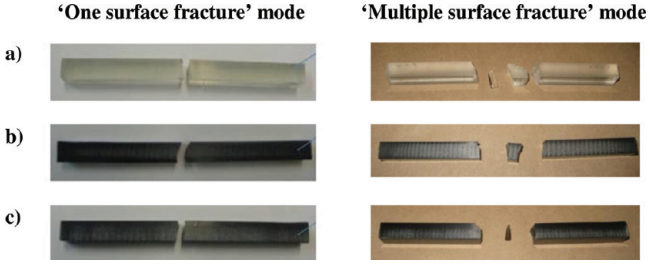

Figure 7. Photographs of the impacted Charpy test specimen: (a) PMMA; (b) PMMA/[raw SWCNT−PMMA]; (c) PMMA/[SWCNT-COOH−PMMA].

Table 6. Charpy Apparent Impact Strength of Selected PMMA/[SWCNT−PMMA] Extruded Composites

sample	apparent impact strength (kJ/m^2)
PMMA	5.0 ± 0.9
PMMA/[raw SWCNT−PMMA]	5.4 ± 0.9
PMMA/[SWCNT-COOH−PMMA]	6.0 ± 1.5

AUTHOR INFORMATION

Corresponding Author
*E-mail: karen.stoeffler@imi.cnrc-nrc.gc.ca.

Notes
The authors declare no competing financial interest.

ACKNOWLEDGMENTS

Funding for this work has been provided by the Chemical, Biological, Radiological-Nuclear, and Explosives Research and Technology Initiative (CRTI). Project CRTI07-121RD. The authors thank C. Kingston and D. Ruth for SWCNT production, J. Guan and H. Dayan for help with SWCNT purification, M. Jakubinek for assistance with Raman mapping analysis, F. Perrin-Sarazin for TEM imaging, and M. Baron (Arkema) for providing the Plexiglas resin.

REFERENCES

(1) Byrne, M.T.; Guin'Ko, Y.K. *Adv. Mater.* **2010**, *22* (15), 1672−1688.
(2) Brown, P; Stevens, K. In *Nanofibers and Nanotechnology in Textiles*; CRC Press: Boca Raton, FL, 2007.
(3) Zhao, W.; Li, M.; Peng, H.-X. *Macromol. Mater. Eng.* **2010**, *295* (9), 838−845.
(4) Bolonkin, A.A. *J. Aerospace Eng.* **2010**, *23* (4), 281−292.
(5) Coleman, J.N.; Khan, U.; Gun'ko, Y.K. *Adv. Mater.* **2006**, *18* (6), 689−706.
(6) Coleman, J.N.; Khan, U.; Blau, W.J.; Gun'ko, Y.K. *Carbon* **2006**, *44* (9), 1624−1652.
(7) Shofner, M.L.; Khabashesku, V.N.; Barrera, E.V. *Chem. Mater.* **2006**, *18* (4), 906−913.
(8) Geng, H.Z.; Rosen, R.; Zheng, B.; Shimoda, H.; Fleming, L.; Liu, J.; Zhou, O. *Adv. Mater.* **2002**, *14* (19), 1387−1390.
(9) Sennett, M.; Welsh, E.; Wright, J.B.; Li, W.Z.; Wen, J.G.; Ren, Z.F. *Appl. Phys. A: Mater. Sci. Process.* **2003**, *76* (1), 111−113.
(10) Treacy, M.M.J.; Ebbesen, T.W.; Gibson, J.M. *Nature* **1996**, *381* (6584), 678−680.
(11) Ebbesen, T.W.; Lezec, H.J.; Hiura, H.; Bennett, J.W.; Ghaemi, H.F.; Thio, T. *Nature* **1996**, *382* (6586), 54−56.
(12) Velasco-Santos, C.; Martinez-Hernandez, A.L.; Castano, V.M. *Compos. Interfaces* **2005**, *11* (8-9), 567−586.
(13) Weon, J.I.; Creasy, T.S.; Sue, H.-J.; Hsieh, A.J. *Polymer Engineering and Science* **2005**, *45* (3), 314−324.
(14) Kingston, C.T.; Jakubek, Z.J.; Dénommée, S.; Simard, B. *Carbon* **2004**, *42* (8-9), 1657−1664.
(15) Talmon, Y.; Pasquali, M. Private communication.
(16) Najafi, E.; Wang, J.; Hitchcock, A.P.; Guan, J.; Dénommée, S.; Simard, B. *J. Am. Chem. Soc.* **2010**, *132* (26), 9020−9029.
(17) Jakubinek, M.B.; Johnson, M.B.; White, M.A.; Guan, J.; Simard, B. *J. Nanosci. Nanotechnol.* **2010**, *10* (12), 8151−8157.
(18) Loos, M.R.; Manas-Zloczower, I. *Macromol. Theory Simul.* **2012**, *21* (2), 130−137.
(19) Du, F.; Scogna, R.C.; Zhou, W.; Brand, S.; Fischer, J.E.; Winey, K.I. *Macromolecules* **2004**, *37* (24), 9048−9055.
(20) Mori, T.; Tanaka, K. *Acta Metall.* **1973**, *21* (5), 571−574.
(21) Mura, T. In *Micromechanics of Defects in Solids*, 2nd ed., revised; Kluwer−Academic: Dordrecht, The Netherlands, 1987.
(22) Popov, V.N.; Van Doren, V.E.; Balkanski, M. *Solid State Commun.* **2000**, *114* (7), 395−399.